Letter

Discovery of 2,4-1H-Imidazole Carboxamides as Potent and Selective TAK1 Inhibitors

Johan J. N. Veerman,* Yorik B. Bruseker, Eddy Damen, Erik H. Heijne, Wendy van Bruggen, Koen F. W. Hekking, Rob Winkel, Christopher D. Hupp, Anthony D. Keefe, Julie Liu, Heather A. Thomson, Ying Zhang, John W. Cuozzo, Andrew J. McRiner, Mark J. Mulvihill, Peter van Rijnsbergen, Birgit Zech, Louis M. Renzetti, Lee Babiss, and Gerhard Müller

ACCESS | Metrics & More | Article Recommendations | SI Supporting Information

7, TAK1 biochemical IC$_{50}$: 1.3 μM
DECL hit

SBDD

54, TAK1 biochemical IC$_{50}$: 0.002 μM
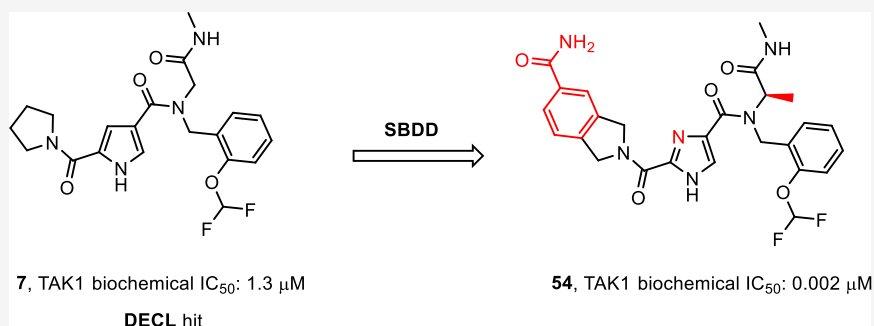
ABSTRACT: Herein we report the discovery of 2,4-1H-imidazole carboxamides as novel, biochemically potent, and kinome selective inhibitors of transforming growth factor β-activated kinase 1 (TAK1). The target was subjected to a DNA-encoded chemical library (DECL) screen. After hit analysis a cluster of compounds was identified, which was based on a central pyrrole-2,4-1H-dicarboxamide scaffold, showing remarkable kinome selectivity. A scaffold-hop to the corresponding imidazole resulted in increased biochemical potency. Next, X-ray crystallography revealed a distinct binding mode compared to other TAK1 inhibitors. A benzylamide was found in a perpendicular orientation with respect to the core hinge-binding imidazole. Additionally, an unusual amide flip was observed in the kinase hinge region. Using structure-based drug design (SBDD), key substitutions at the pyrrolidine amide and the glycine resulted in a significant increase in biochemical potency.

KEYWORDS: Kinase, TAK1, MAP3K7, DNA-encoded chemical library (DECL), Structure-based drug design (SBDD)

The mitogen-activated protein kinase (MAPK) pathways consist of multiple conserved kinases, ultimately linking extracellular signals to crucial intracellular processes, and deregulation of its members has potential implications in both inflammatory[1] and oncological disorders.[2,3] After first being reported in 1995,[4] the transforming growth factor β-activated kinase 1 (TAK1, MAP3K7) has in fact emerged as a potential therapeutic target for both inflammatory diseases and cancer.[5,6] TAK1 is activated by transforming growth factor-β (TGF- β) and facilitates downstream signaling of multiple pro-inflammatory cytokines such as TNF-α, TLR ligands, LPS, and IL-1.[7–10] Although the complex mechanisms through which TAK1 activation and signaling are controlled have not been fully elucidated, it has been recognized that TAK1 phospho-activates members of the MAP2K family, including MKK3/4/6/7, as well as IKK kinases, both of which are in turn activators of the downstream MAP kinases p38 and JNK and the transcription factor NFkB.[11–13] Through activation of these pathways, TAK1 has a pro-survival role, by inducing expression

of antiapoptotic proteins and cytokines, thus inhibiting apoptosis and promoting cell proliferation.[14–16] Specifically, it has been demonstrated that inhibition of TAK1 activity sensitized tumor cells to TRAIL-induced apoptosis.[17] Moreover, the therapeutic potential of TAK1 inhibitors has been investigated for the treatment of pancreatic,[18] ovarian,[19] and breast[20] cancers as well as in inflammatory diseases.[21]
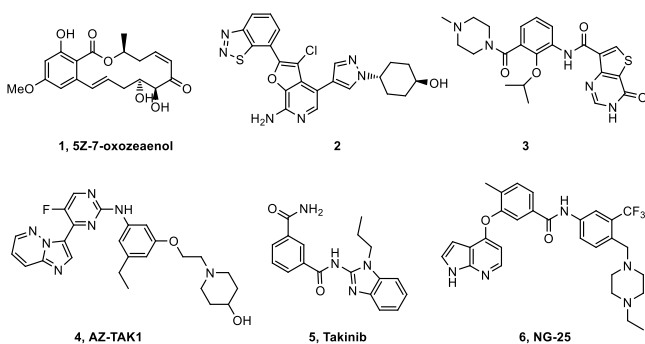
The first inhibitors described for TAK1 exploit the active site cysteine residue found in this kinase, and the most extensively studied example of these is the natural product 5Z-7-oxozeaenol **1**[22,23] (Figure 1). This compound binds to the hinge with the phenol and reaction of the enone with a

Figure 1. Structures of TAK1 inhibitors.

cysteine in the active site results in the formation of a covalent bond leading to irreversible inhibition of the enzyme. The compound was shown to be active in cells, but as many other kinases have a similarly located cysteine, the compound may not be very selective. More recently, both type I ATP hinge-binding inhibitors and type II DFG-out inhibitors have been described. Compound **2**[24,25] is the result of a program pursued at OSI Pharmaceuticals, where the aminopyridine is binding to the hinge and the benzothiadiazole is forming an interaction with the catalytic lysine in the phosphate pocket. The compound showed good selectivity in a screen against 192 kinases and was found to be active in cells and in a mouse tumor xenograft model. Another type I inhibitor was developed by Chugai Pharmaceuticals. Optimization of a screening hit using SBDD resulted in compound **3**.[26] The inhibitor showed good activity and excellent selectivity. Unfortunately, poor cell activity was observed due to poor permeability. In a very nice display of SBDD using crystal structure overlays, the compound was converted into both DFG-out and c-helix-out type II inhibitors.[27] The potential role of a TAK1 inhibitor **AZ-TAK1** (**4**)[28] in mantle cell lymphoma was described by Bugli et al. The compound was potent, but it was fairly unselective with an IC_{50} below 100 nM for 10 out of 30 enzymes in a small kinase panel. Recently, Takinib (**5**)[29] was described to inhibit TAK1 selectively, resulting in TNF-α induced apoptosis. Finally, type II inhibitors have also been described for TAK1, such as **NG-25** (**6**)[30] as developed by Gray et al.

In a program to identify novel and structurally distinct inhibitors of TAK1, we subjected the target to a DECL screen.[31] Briefly, twenty-one different DNA-encoded chemical libraries were combined and this mixture was incubated with TAK1−TAB1 fusion protein. Separate incubations were set up with no target, TAK1−TAB1 at 7.8 μM, TAK1−TAB1 at 1.6 μM, and with TAK1−TAB1 at 7.8 μM and 5Z-7-oxozeaenol (**1**) at 40 μM. After a 1 h of incubation the mixtures were captured on the His-Select IMAC matrix, washed, and then heat-eluted at 85 °C. A second round of selection was performed using the round-one eluate as input and fresh proteins and **1** repeating the conditions of the first round. The encoding DNA in the output of the second round of selection was amplified, and the amplified sample was submitted for sequencing using an Illumina 2500 instrument in high-output mode. Ninety-seven million single-end reads were generated across all twenty-one libraries for these four selections. Sequence data were parsed, and each read was assigned to the library chemical scheme and the specific building blocks used to synthesize it and the experimental condition it was subjected to during selection. Statistical and demographic data

were calculated for all building block combinations. One of the compounds prioritized for resynthesis was derived from a library which had been synthesized by installing 940 unique primary amines onto a DNA-linked aldehyde followed by reaction with 4,000 capping reagents including carboxylic acids and other secondary amine-reactive building blocks. This library contains 3.76 million different compounds, each of which is encoded by a unique DNA tag combination. This cluster of structurally related compounds was defined by the capping building block—(pyrrolidine-1-carbonyl)-1*H*-pyrrole-3-carboxylic acid—and was coenriched with a range of 2-substituted phenyl methanamines with 2-(difluoromethoxy-phenyl)methanamine being the most enriched. These compounds showed a complete absence of enrichment in the selection with TAK1-TAB1 and a saturating concentration of 5Z-7-oxozeaenol, consistent with the hypothesis that their binding sites on the target protein overlap. It was this most enriched combination of building blocks that was chosen for resynthesis of the initial hit compound, compound **7** (Figure 2), along with the first few atoms of what during the screen was the linker to the encoding DNA.
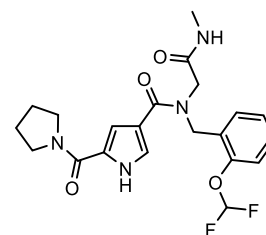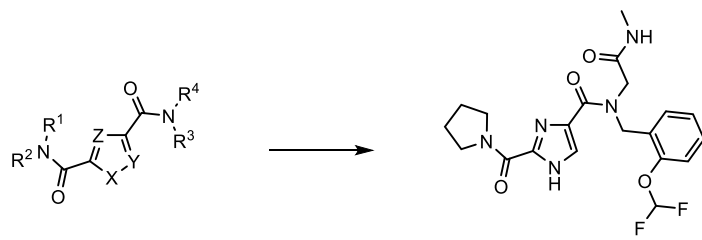

7, TAK1 biochemical IC_{50}: 1.3 μM

Figure 2. Primary hit compound **7**.

The primary hits were verified by synthesis of the label free analogs and subjected to a kinase inhibition assay. A LanthaScreen biochemical kinase inhibition assay using TAK1-TAB1 fusion protein in the presence of 10 μM ATP was used to assess the potency of the compounds. As a positive control Staurosporine was used and this had an IC_{50} value of 39 nM. To compare to known TAK1 inhibitors, the biochemical potency of compounds **2** and **3** was determined under these conditions. Compound **2** was found to have an IC_{50} value of 10 nM, which is lower than the 28 nM IC_{50} value reported,[24] where an AlphaScreen biochemical assay was used in the presence of 100 μM ATP. Compound **3** had an IC_{50} value of 30 nM, where an IC_{50} value of 11 nM was reported[26] using a radiometric biochemical kinase assay. In this assay, compound **7** (Figure 2) showed a biochemical IC_{50} value of 1.3 μM and it was used as a starting point for interrogating R^1 to R^4 and the pyrrole core in order to generate SAR (Table 1, compound **8**). Although we had no structural information at this point, we assumed a type I binding mode, based on the binding modes described for compounds **2** and **3**. We envisioned the pyrrolidine making hydrophobic interactions in the back of the pocket, the amide ketone and the pyrrole NH making hydrogen bond interactions with the hinge region of the kinase, and the *N*-methyl amide pointing to the solvent as this was the attachment point for the DNA tag. Indeed, structural changes at the DNA-linker region R^4 (compounds **9**−**12**) did not influence potency much, with IC_{50} values ranging from 0.9 to 3.5 μM. Some additional ortho-substituted benzyl amine derivatives (R^3) were synthesized, but flat SAR

**Table 1. In Vitro Biochemical Potency Data for Initial Derivatives of Compound 7**

Sol: 30 μM (PBS buffer, pH 7.4)
S9 Microsomal stability (H/M/R): $t_{1/2}$ >2 h
Caco2 (A>B/B>A): 1/20 (10^{-6} cms^{-1})

8

22, TAK1 biochemical IC$_{50}$: 0.6 μM, Kd: 52 nM

Compd	R^1, R^2N	R^3	R^4	X, Y, Z	TAK1 IC$_{50}$[a]
9	1-pyrrolidinyl	2-(OCHF$_2$)benzyl	2-amino-2-oxoethyl	N, CH, CH	0.9
10	1-pyrrolidinyl	2-(OCHF$_2$)benzyl	2-(isopropylamino)-2-oxoethyl	N, CH, CH	1.7
11	1-pyrrolidinyl	2-(OCHF$_2$)benzyl	oxazol-2-ylmethyl	N, CH, CH	3.2
12	1-pyrrolidinyl	2-(OCHF$_2$)benzyl	methyl	N, CH, CH	3.5
13	1-pyrrolidinyl	2-(OMe)benzyl	2-(methylamino)-2-oxoethyl	N, CH, CH	2.8
14	1-pyrrolidinyl	2-(OEt)benzyl	2-(methylamino)-2-oxoethyl	N, CH, CH	2.6
15	1-pyrrolidinyl	(3,4-dihydro-2H-benzo[b][1,4]dioxepin-6-yl)methyl	2-(methylamino)-2-oxoethyl	N, CH, CH	3.4
16	1-pyrrolidinyl	(1H-indol-4-yl)methyl	2-(methylamino)-2-oxoethyl	N, CH, CH	1.8
17	N,N-dimethyl	2-(OCHF$_2$)benzyl	2-(methylamino)-2-oxoethyl	N, CH, CH	26
18	1-piperidinyl	2-(OCHF$_2$)benzyl	2-(methylamino)-2-oxoethyl	N, CH, CH	1.8
19	N-ethyl	2-(OCHF$_2$)benzyl	2-(methylamino)-2-oxoethyl	N, CH, CH	>100
20	1-pyrrolidinyl	2-(OCHF$_2$)benzyl	2-(methylamino)-2-oxoethyl	N, N, CH	59
21	1-pyrrolidinyl	2-(OCHF$_2$)benzyl	2-(methylamino)-2-oxoethyl	NMe, CH, CH	>100

[a]Biochemical Lanthascreen assay with TAK1−TAB1 fusion protein in the presence of 10 μM ATP, mean IC$_{50}$ values in μM, $n = 2$.

Scheme 1. Synthetic Routes (A, B) for the Synthesis of 2,4-1H-Imidazole Carboxamides[a]
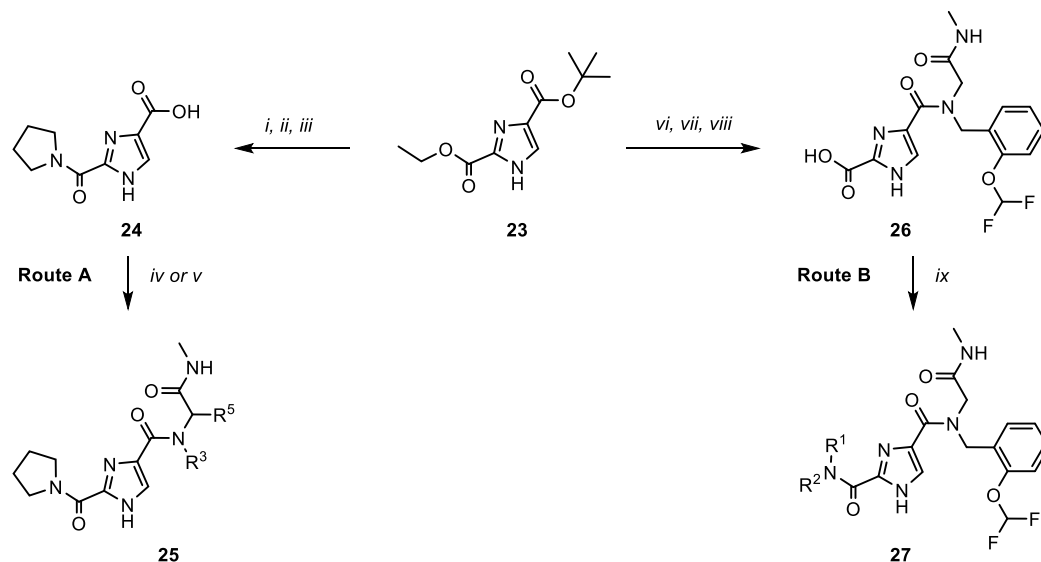
[a]Reagents and conditions: [i] LiOH, THF/H$_2$O, RT, 16 h; [ii] pyrrolidine, HATU, DMF, RT, 16 h, 36% over two steps; [iii] formic acid, CHCl$_3$, 2 h, reflux, 95%; [iv] amine, HATU, Et$_3$N, DMF, RT, 16 h, 20−67%; [v] R^{3}NH$_2$, R^{5}CHO, methylisocyanide, MeOH, RT, 16 h, 9−64%; [vi] formic acid, CHCl$_3$, 2 h, reflux, 88%; [vii] 2-((2-(difluoromethoxy)benzyl)amino)-N-methylacetamide, HATU, Et$_3$N, DMF, RT, 16 h, 77%; [viii] LiOH, THF/H$_2$O, 40 °C, 16 h, 98%; [ix] R^{1}R^{2}NH, HATU, Et$_3$N, DMF, RT, 16 h, 18−80%.

was observed for compounds 13−16, indicating that there was some room for larger substituents at that position. Next, the pyrrolidine moiety was varied. Interestingly, the corresponding dimethyl analog 17 showed a 20-fold drop in potency, while the piperidine amide 18 retained significant potency, which suggested steric repulsion. The more polar primary amide 19 was completely inactive, possibly caused by hydrophobic repulsion. Apparently, this amide is involved in positioning key interactions with the target kinase. Finally, some changes to the core pyrrole were made. The pyrazole derivative 20 showed a
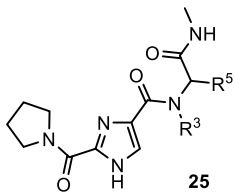
large drop in potency. Methylation of the nitrogen gave derivative 21, which was inactive. Interestingly, imidazole 22 resulted in a 2-fold increase in potency. This steep SAR suggested that the core is of prime importance for inhibitory activity, rather than just being a scaffold with orientation function for the peripheral R-groups and would be consistent with the assumption it was making hydrogen bond interactions with the hinge of the kinase. As the imidazole showed promising potency, additional assay data were collected. The K_d was determined to be 55 nM (KdELECT, DiscoverX). The

compound had a 30 μM solubility in PBS buffer and showed good metabolic stability in microsome assays. A Caco-2 assay showed low A to B permeability and an efflux ratio of 20. Most striking was the selectivity profile of imidazole **22**. Upon screening at 10 μM in a 468 kinase panel containing 453 human and 403 wildtype kinases (KINOMEscan, DiscoverX), only 4 additional kinases were inhibited >65%: ABL1(H369P), EIF2AK1, TNK2, and YANK1. No other kinases in the TKL subfamily were inhibited. As we were expecting the selectivity to change during the optimization of the compound, we did not further investigate these off-targets. Assuming a type I binding mode, it is hard to explain this selectivity as the molecule is relatively small. At that point, **22** became our front-runner compound.

As the imidazole core was readily accessible and easily amenable to synthetic derivatization, a targeted library approach was initiated to further explore the potential of compound **22** (Scheme 1). For this purpose, the diester **23** was synthesized on multigram scale as an advanced intermediate.[32] The orthogonally protected esters conveniently allowed for stepwise derivatization and synthesis of a plethora of analogs. Two routes were devised toward the desired products. Basic hydrolysis of the ethyl ester, followed by pyrrolidine coupling and acid induced deprotection, afforded key building block **24**. The carboxylic acid was then converted to amides **25** by coupling with an amine or via an Ugi multicomponent reaction (**Route A**). Alternatively, the *t*Bu ester was deprotected and converted into the amide, followed by hydrolysis of the ethyl ester to afford intermediate **26**. This was then converted into the amide to afford products **27** (**Route B**).

With the chemistry set up, a closer look was taken at the *N*-benzyl group (R^3) and the glycine (R^5) moiety (Table 2) and a small diversity set was made. Introduction of an α-methyl on the benzyl (**28**) abolished the activity, possibly caused by

changing the orientation of the benzyl group. Removal of or shifting the $OCHF_2$ group (**29**, **30**) also rendered the compound to be inactive, indicating that this group makes an essential interaction. While keeping the 2-$OCHF_2$ on the benzyl in place, additional substitution on the benzyl ring was investigated. It turned out the phenyl ring was sensitive toward further substitution. Introduction of a methoxy group on the 3- (**31**) or 4-postion (**32**) as well as fluorination or chlorination on the 5- (**33**, **34**) or 6-position (**35**, **36**) resulted in inactive compounds, suggesting steric occlusion. Next, substitution on the glycine carbon was investigated. Introduction of a methyl was allowed and the compound retained potency (**37**), while larger groups like an ethyl (**38**) or 2-propyl (**39**) resulted in loss of potency. The enantiomers of **37** were synthesized separately, and it was found that the *R*-enantiomer **40** was considerably more active than the *S*-enantiomer **41**, effectively increasing the potency of compound **22** by a factor of 2. This difference was hard to explain without structural information, but suggested limited room at that position with the *S*-methyl making an unfavorable interaction. As the pyrrolidine amide was also found to be sensitive to changes in the first hit expansion campaign, this moiety was further probed. First, the ring size was investigated (Table 3). Change of the pyrrolidine

Table 3. In Vitro Potency Data for Compounds 42−52

Compd	R^1R^2N	TAK1 IC50^a
42	1-azetidinyl	2.6
43	1-piperidinyl	1.2
44	1-azepinyl	2.9
45	1-(2-methylpyrrolidinyl)	5.7
46	1-(3-methylpyrrolidinyl)	0.9
47	1-(3-fluoropyrrolidinyl)	1.2
48	1-(3-phenylpyrrolidinyl)	2.3
49	1-(3-(OMe)-pyrrolidinyl)	>10
50	1-(3-(*N*-Ac)-pyrrolidinyl)	>10
51	1-isoindolinyl	0.3
52	1-octahydro-1*H*-isoindolinyl	3.4

^{a}Biochemical Lanthascreen assay with TAK1−TAB1 fusion protein in the presence of 10 μM ATP, mean IC_{50} values in μM, n = 2.

for a smaller azetidine resulted in a 4-fold drop in potency (**42**). Ring expansion to a 6- (**43**) or 7-membered ring (**44**) resulted in a slight drop in potency, indicating limited room as was also observed for the pyrrole analogs **17** and **18**. As the pyrrolidine **22** showed the best biochemical potency, substitution on the five-membered ring was probed. Introduction of a 2-methyl resulted in a large drop in potency (**45**) indicating steric congestion, but substitution on the 3-position of the pyrrolidine was tolerated. Lipophilic groups like fluoro, methyl, or phenyl groups retained potency (**46−48**), but more polar moieties like a methoxy (**49**) or an *N*-acetyl (**50**) resulted in loss of potency, which is consistent with the hydrophobic nature of the residues in the back part of the pocket. Interestingly, an isoindoline (**51**) yielded a 2-fold

Table 2. In Vitro Potency Data for Compounds 28−41

Compd	R^3	R^5	TAK1 IC_{50}^{a}
28	α-methyl-2-($OCHF_2$)benzyl	H	>10
29	benzyl	H	>10
30	3-($OCHF_2$)benzyl	H	>10
31	2-($OCHF_2$)-3-(OMe)benzyl	H	>10
32	2-($OHCF_2$)-4-(OMe)benzyl	H	>10
33	2-($OCHF_2$)-5-fluorobenzyl	H	>10
34	2-($OCHF_2$)-5-chlorobenzyl	H	>10
35	2-($OCHF_2$)-6-fluorobenzyl	H	>10
36	2-($OCHF_2$)-6-chlorobenzyl	H	>10
37	2-($OCHF_2$)benzyl	Me	0.5
38	2-($OCHF_2$)benzyl	Et	1.0
39	2-($OCHF_2$)benzyl	*i*Pr	>10
40	2-($OCHF_2$)benzyl	*R*-Me	0.3
41	2-($OCHF_2$)benzyl	*S*-Me	4.5

^{a}Biochemical Lanthascreen assay with TAK1−TAB1 fusion protein in the presence of 10 μM ATP, mean IC_{50} values in μM, n = 2.

increase in potency, but the corresponding fully reduced form lost 10-fold in activity (**52**), again indicating steric congestion.

Having made only moderate gains in potency, further guidance for compound optimization needed to be obtained from structural information. At this point a crystal structure of compound **22** bound to TAK1 was acquired (Figure 3, top).
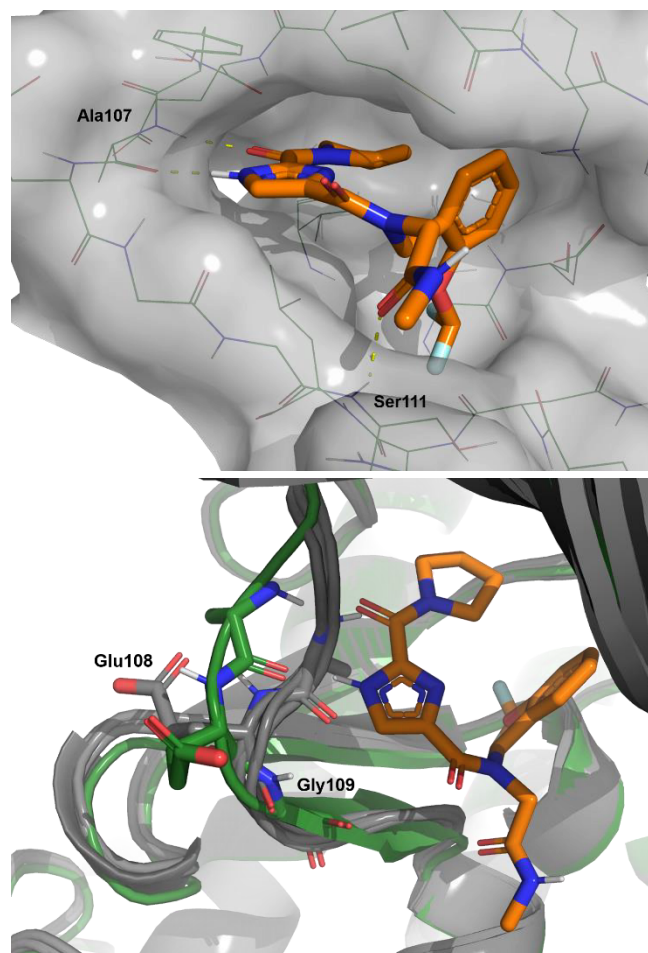
Figure 3. (Top) Detailed view of compound **22** bound to the ATP binding site of TAK1. (Bottom) Overlay of several X-rays of TAK1 with type-I binding compounds (gray) (PDB ID codes: 2EVA, 4L53, 5JGD, and 5V5N) and compound **22** structure (green).

The structure confirmed binding to the hinge in a type-I fashion and showed the imidazole and the carbonyl to bind as a donor−acceptor pair with the backbone functionalities of Ala107. As envisioned, the pyrrolidine is pointing to the back, and now the SAR observed for this moiety can be rationalized. There is no room for substitution of the 2-position, and it is clear why substitution at the 3-position is allowed, with more lipophilic residues (**46**−**48**, **51**) retaining potency as this part of the pocket contains mainly aliphatic residues. The glycine carbonyl makes an interaction at the edge of the pocket with the amine hydrogen of Ser111. Finally, the orientation of the benzyl group is observed to be perpendicular to the imidazole core with the $OCHF_2$ moiety nicely filling up a small lipophilic subpocket and the phenyl group making a lipophilic interaction. This explains the steep SAR observed for compounds **28**−**36** as removal of the $OCHF_2$ or substitution of the phenyl would thwart these interactions. Additionally, the difference observed between the *R*- and *S*-enantiomers **40** and
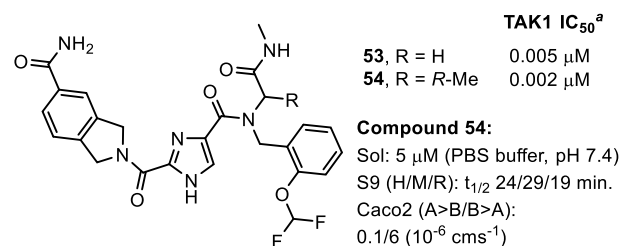
41 can be explained. The *R*-methyl would fit, whereas the *S*-methyl would result in a steric clash with the protein. As the most striking observation, an overlay of the structure with some examples of crystal structures of other type-I TAK1 inhibitors showed this to be a unique binding mode for TAK1 (Figure 3, bottom). In the hinge region a peptide flip occurs between Glu108 and Gly109, thereby moving the backbone trace of the hinge when compared to the structures of other type-I inhibitors bound to TAK1. These conformational differences of the TAK1 protein induced by compound **22** potentially contribute to the observed selectivity in the kinase panel.[33,34] With the structure in hand, a rational design campaign was enabled. For compounds **2** and **3**, structures were reported and both papers stated a jump in potency was reached by targeting the Lys63-Asp175 pair. An overlay of these structures with the compound **22** structure (Figures 4
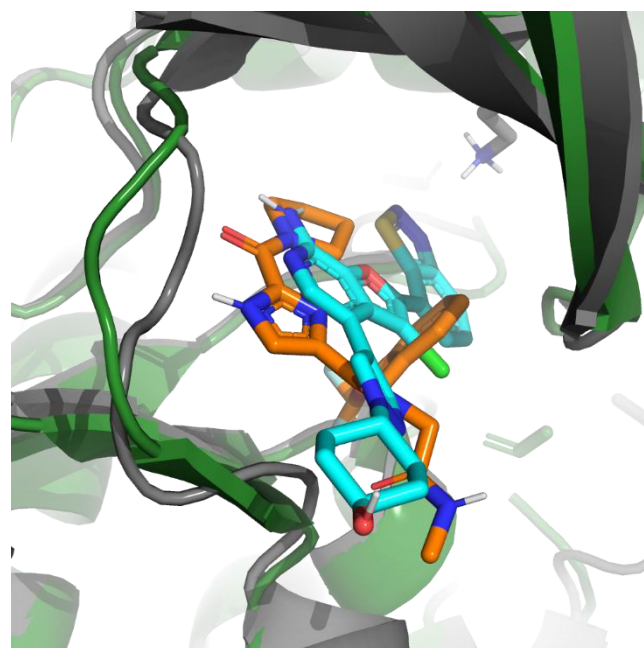
Figure 4. Overlay of the structures of compound **22** (orange and green) with **2** (gray and cyan, PDB ID code: 4L53). Key lysine residue depicted.

and S-1) suggested we should be able to target this interaction from the pyrrolidine. Docking indicated the isoindoline **51** to be a suitable platform for this and compound **53** was synthesized (Figure 5).

Gratifyingly, a >100-fold jump in biochemical potency compared to **22** was obtained. Additionally, selectivity was

	TAK1 IC$_{50}$[a]
53, R = H	0.005 μM
54, R = *R*-Me	0.002 μM

Compound **54**:
Sol: 5 μM (PBS buffer, pH 7.4)
S9 (H/M/R): $t_{1/2}$ 24/29/19 min.
Caco2 (A>B/B>A):
0.1/6 (10^{-6} cms^{-1})

Figure 5. Compounds **53** and **54**. [a] Biochemical Lanthascreen assay with TAK1−TAB1 fusion protein in the presence of 10 μM ATP, mean IC$_{50}$ values in μM, *n* = 2.

maintained; in a screen at 1 μM in a 468 kinase panel, apart from TAK1, only 6 additional kinases were inhibited >65%: CSNK2A1, SCNK2A2, FLT3(D835 V), PFCDPK1, PIK3CD, and PIP5K1C. Interestingly, none of these kinases were inhibited by compound **22** and selectivity in the TKL family was retained. Finally, addition of the privileged *R*-methyl group onto the glycine resulted in compound **54**, with a 2 nM TAK1 biochemical IC_{50} value, which marks the detection limit of the biochemical assay. A crystal structure was obtained for compound **54** that confirmed the binding mode (Figure 6).
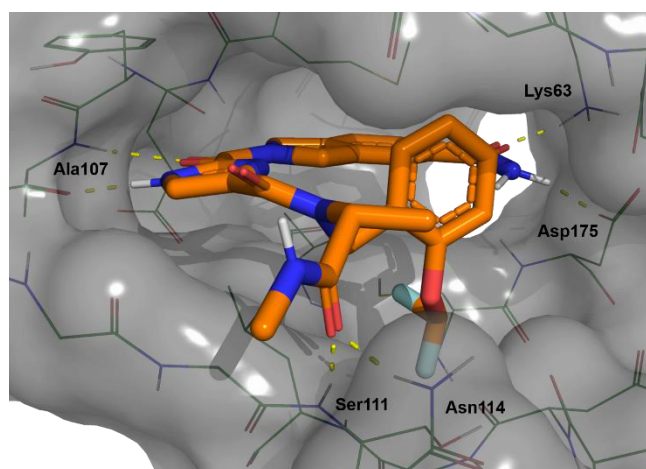
Figure 6. Detailed view of compound **54** bound to the ATP binding site of TAK1.

The isoindoline carboxamide showed a dual interaction with Lys63 as well as the Asp175. Again, the hinge was moved as was observed in the first structure. To assess the potency in a cellular context, TNF-α stimulated HCT-15 cells were treated with compound **54** to determine its effect on cell viability, but no effect was observed using concentrations up to 10 μM, whereas control compound **1** showed an EC_{50} value of 2 nM. Some additional ADME parameters were collected for **54**. Compared to **22**, the solubility of **54** had dropped 6-fold and introduction of additional substituents resulted in a decrease in metabolic stability as observed in the S9 microsome stability assay. Finally, the permeability was checked using a Caco-2 assay and A to B permeability had dropped to 0.1×10^{-6} cms^{-1}, which could explain the results observed in the cell based assay.

In conclusion, a DECL library hit against TAK1 was found and partially optimized by a library approach. Next, the binding mode was determined by X-ray and the potency was improved using SBDD. The resulting compound **54** has good biochemical potency and kinome selectivity, but the physchem properties need further optimization, which will be reported in due course.

■ ASSOCIATED CONTENT

Ⓢ Supporting Information

The Supporting Information is available free of charge at https://pubs.acs.org/doi/10.1021/acsmedchemlett.0c00547.

> Experimental procedures for the synthesis of compounds **7**−**24**, **26**, and **28**−**54**. A description of the biochemical, cell, solubility, S9 and permeability assays, DECL-screen, crystallization conditions, kinase panel data and Supplementary Figure **S-1** (PDF)

■ AUTHOR INFORMATION

Corresponding Author

Johan J. N. Veerman − *ZoBio BV, 2333 CH Leiden, The Netherlands;* ⓞ orcid.org/0000-0001-8266-4721; Email: jveerman@zobio.com

Authors

Yorik B. Bruseker − *Mercachem BV, Department of Medicinal Chemistry, 6546 BB Nijmegen, The Netherlands*

Eddy Damen − *Mercachem BV, Department of Medicinal Chemistry, 6546 BB Nijmegen, The Netherlands*

Erik H. Heijne − *Mercachem BV, Department of Medicinal Chemistry, 6546 BB Nijmegen, The Netherlands;* ⓞ orcid.org/0000-0002-1288-8540

Wendy van Bruggen − *Mercachem BV, Department of Medicinal Chemistry, 6546 BB Nijmegen, The Netherlands*

Koen F. W. Hekking − *Mercachem BV, Department of Medicinal Chemistry, 6546 BB Nijmegen, The Netherlands*

Rob Winkel − *Mercachem BV, Department of Medicinal Chemistry, 6546 BB Nijmegen, The Netherlands*

Christopher D. Hupp − *X-Chem, Inc., Waltham, Massachusetts 02453, United States*

Anthony D. Keefe − *X-Chem, Inc., Waltham, Massachusetts 02453, United States*

Julie Liu − *Civetta Therapeutics, Cambridge, Massachusetts 02138, United States*

Heather A. Thomson − *X-Chem, Inc., Waltham, Massachusetts 02453, United States*

Ying Zhang − *X-Chem, Inc., Waltham, Massachusetts 02453, United States*

John W. Cuozzo − *X-Chem, Inc., Waltham, Massachusetts 02453, United States;* ⓞ orcid.org/0000-0002-6229-0395

Andrew J. McRiner − *X-Chem, Inc., Waltham, Massachusetts 02453, United States*

Mark J. Mulvihill − *HiberCell Inc., New York 10019, United States*

Peter van Rijnsbergen − *Mercachem BV, Department of Medicinal Chemistry, 6546 BB Nijmegen, The Netherlands*

Birgit Zech − *AnavoTherapeutics BV, 2333 CH Leiden, The Netherlands*

Louis M. Renzetti − *Bridge Medicines LLC, New York 10017, United States*

Lee Babiss − *Wilmington, North Carolina 28405, United States*

Gerhard Müller − *AnavoTherapeutics BV, 2333 CH Leiden, The Netherlands*

Complete contact information is available at: https://pubs.acs.org/10.1021/acsmedchemlett.0c00547

Notes

The authors declare no competing financial interest.
The structures of **TAK1:22** and **TAK1:54** will be released upon publication.

■ ABBREVIATIONS

TAK1, transforming growth factor β-activated kinase 1; DECL, DNA-encoded chemical library; SBDD, structure based drug design; TGF-β, transforming growth factor-β; TNF-α, tumor necrosis factor alpha; TLR, Toll-like receptor; LPS, lipopolysaccharide; IL-1, interleukin 1; TAB, TAK1-binding protein; MAP, mitogen-activated protein; NFkB, nuclear factor-κB; TRAIL, TNF-related apoptosis-inducing ligand;

ATP, adenosine triphosphate; SAR, structure−activity relationship; RT, room temperature; HATU, (1-[Bis(dimethylamino)-methylene]-1*H*-1,2,3-triazolo[4,5-*b*]pyridinium 3-oxide hexafluorophosphate; Et$_3$N, triethylamine

■ REFERENCES

(1) Arthur, J. S. C.; Ley, S. C. Mitogen-activated protein kinases in innate immunity. *Nat. Rev. Immunol.* **2013**, *13*, 679−692.

(2) Burotto, M.; Chiou, V. L.; Lee, J.-M.; Kohn, E. C. The MAPK pathway across different malignancies: a new perspective. *Cancer* **2014**, *120*, 3446−3456.

(3) Dhillon, A. S.; Hagan, S.; Rath, O.; Kolch, W. MAP kinase signalling pathways in cancer. *Oncogene* **2007**, *26*, 3279−3290.

(4) Yamaguchi, K.; Shirakabe, K.; Shibuya, H.; Irie, K.; Oishi, I.; Ueno, N.; Taniguchi, T.; Nishida, E.; Matsumoto, K. Identification of a member of the MAPKKK family as a potential mediator of TGF-beta signal transduction. *Science* **1995**, *270*, 2008−2011.

(5) Sakurai, H. Targeting of TAK1 in inflammatory disorders and cancer. *Trends Pharmacol. Sci.* **2012**, *33*, 522−530.

(6) Kilty, I.; Jones, L. H. TAK1 selective inhibition: state of the art and future opportunities. *Future Med. Chem.* **2015**, *7*, 23−33.

(7) Sakurai, H.; Shigemori, N.; Hasegawa, T.; Sugita, T. TGF-beta-activated kinase 1 stimulates NF-kappa B activation by an NF-kappa B-inducing kinase-independent mechanism. *Biochem. Biophys. Res. Commun.* **1998**, *243*, 545−549.

(8) Shirakabe, K.; Yamaguchi, K.; Shibuya, H.; Irie, K.; Matsuda, S.; Moriguchi, T.; Gotoh, Y.; Matsumoto, K.; Nishida, E. TAK1Mediates the Ceramide Signaling to Stress-activated Protein Kinase/c-Jun N-terminal Kinase. *J. Biol. Chem.* **1997**, *272*, 8141−8144.

(9) Sakurai, H.; Miyoshi, H.; Toriumi, W.; Sugita, T. Functional interactions of transforming growth factor beta-activated kinase 1 with IkappaB kinases to stimulate NF-kappaB activation. *J. Biol. Chem.* **1999**, *274*, 10641−10648.

(10) Ninomiya-Tsuji, J.; Kishimoto, K.; Hiyama, A.; Inoue, J.; Cao, Z.; Matsumoto, K. The kinase TAK1 can activate the NIK-I kappaB as well as the MAP kinase cascade in the IL-1 signalling pathway. *Nature* **1999**, *398*, 252−256.

(11) Adhikari, A.; Xu, M.; Chen, Z. J. Ubiquitin-mediated activation of TAK1 and IKK. *Oncogene* **2007**, *26*, 3214−3226.

(12) Shibuya, H.; Yamaguchi, K.; Shirakabe, K.; Tonegawa, A.; Gotoh, Y.; Ueno, N.; Irie, K.; Nishida, E.; Matsumoto, K. TAB1: An Activator of the TAK1MAPKKK in TGF-*β* Signal Transduction. *Science* **1996**, *272*, 1179−1182.

(13) Takaesu, G.; Kishida, S.; Hiyama, A.; Yamaguchi, K.; Shibuya, H.; Irie, K.; Ninomiya-Tsuji, J.; Matsumoto, K. TAB2, a novel adaptor protein, mediates activation of TAK1MAPKKK by linking TAK1 to TRAF6 in the IL-1 signal transduction pathway. *Mol. Cell* **2000**, *5*, 649−658.

(14) Mihaly, S. R.; Ninomiya-Tsuji, J.; Morioka, S. TAK1 control of cell death. *Cell Death Differ.* **2014**, *21*, 1667−1676.

(15) Hayden, M. S.; Ghosh, S. Shared principles in NF-*κ*B signaling. *Cell* **2008**, *132*, 344−362.

(16) Wang, Z.; Zhang, W.; Shi, M.; Yu, Y.; Wang, H.; Cao, W.-M.; Zhao, Y.; Zhang, H. TAK1 inhibitor NG25 enhances doxorubicin-mediated apoptosis in breast cancer cells. *Sci. Rep.* **2016**, *6*, 32737.

(17) Choo, M.-K.; Kawasaki, N.; Singhirunnusorn, P.; Koizumi, K.; Sato, S.; Akira, S.; Saiki, I.; Sakurai, H. Blockade of transforming growth factor-beta-activated kinase 1 activity enhances TRAIL-induced apoptosis through activation of a caspase cascade. *Mol. Cancer Ther.* **2006**, *5*, 2970−2976.

(18) Melisi, D.; Xia, Q.; Paradiso, G.; Ling, J.; Moccia, T.; Carbone, C.; Budillon, A.; Abbruzzese, J. L.; Chiao, P. J. Modulation of pancreatic cancer chemoresistance by inhibition of TAK1. *J. Natl. Cancer Inst.* **2011**, *103*, 1190−1204.

(19) Ying, L.; Chunxia, Y.; Wei, L. Inhibition of ovarian cancer cell growth by a novel TAK1 inhibitor LYTAK1. *Cancer Chemother. Pharmacol.* **2015**, *76*, 641−650.

(20) Zonneville, J.; Wong, V.; Limoge, M.; Nikiforov, M.; Bakin, A. V. TAK1 signaling regulates p53 through a mechanism involving ribosomal stress. *Sci. Rep.* **2020**, *10*, 2517.

(21) Scarneo, S. A.; Mansourati, A.; Eibschutz, L. S.; Totzke, J.; Roques, J. R.; Loiselle, D.; Carlson, D.; Hughes, P.; Haystead, T. A. J. Genetic and pharmacological validation of TAK1 inhibition in macrophages as a therapeutic strategy to effectively inhibit TNF secretion. *Sci. Rep.* **2018**, *8*, 17058.

(22) Ninomiya-Tsuji, J.; Kajino, T.; Ono, K.; Ohtomo, T.; Matsumoto, M.; Shiina, M.; Mihara, M.; Tsuchiya, M.; Matsumoto, K. A resorcylic acid lactone, 5Z-7-oxozeaenol, prevents inflammation by inhibiting the catalytic activity of TAK1MAPK kinase kinase. *J. Biol. Chem.* **2003**, *278*, 18485−18490.

(23) Wu, J.; Powell, F.; Larsen, N. A.; Lai, Z.; Byth, K. F.; Read, J.; Gu, R. F.; Roth, M.; Toader, D.; Saeh, J. C.; Chen, H. Mechanism and In Vitro Pharmacology of TAK1 Inhibition by (5Z)-7-Oxozeaenol. *ACS Chem. Biol.* **2013**, *8*, 643−650.

(24) Hornberger, K. R.; Chen, X.; Crew, A. P.; Kleinberg, A.; Ma, L.; Mulvihill, M. J.; Wang, J.; Wilde, V. L.; Albertella, M.; Bittner, M.; Cooke, A.; Kadhim, S.; Kahler, J.; Maresca, P.; May, E.; Meyn, P.; Romashko, D.; Tokar, B.; Turton, R. Discovery of 7-aminofuro[2,3-c]pyridine inhibitors of TAK1: optimization of kinase selectivity and pharmacokinetics. *Bioorg. Med. Chem. Lett.* **2013**, *23*, 4511−4516.

(25) Hornberger, K. R.; Berger, D. M.; Crew, A. P.; Dong, H.; Kleinberg, A.; Li, A.-H.; Medeiros, M. R.; Mulvihill, M. J.; Siu, K.; Tarrant, J.; Wang, J.; Weng, F.; Wilde, V. L.; Albertella, M.; Bittner, M.; Cooke, A.; Gray, M. J.; Maresca, P.; May, E.; Meyn, P.; Peick, W., Jr.; Romashko, D.; Tanowitz, M.; Tokar, B. Discovery and optimization of 7-aminofuro[2,3-c]pyridine inhibitors of TAK1. *Bioorg. Med. Chem. Lett.* **2013**, *23*, 4517−4522.

(26) Muraoka, T.; Ide, M.; Morikami, K.; Irie, M.; Nakamura, M.; Miura, T.; Kamikawa, T.; Nishihara, M.; Kashiwagi, H. Discovery of a potent and highly selective transforming growth factor *β* receptor-associated kinase 1 (TAK1) inhibitor by structure based drug design (SBDD). *Bioorg. Med. Chem.* **2016**, *24*, 4206−4217.

(27) Muraoka, T.; Ide, M.; Irie, M.; Morikami, K.; Miura, T.; Nishihara, M.; Kashiwagi, H. Development of a Method for Converting a TAK1 Type I Inhibitor into a Type II or c-Helix-Out Inhibitor by Structure-Based Drug Design (SBDD). *Chem. Pharm. Bull.* **2016**, *64*, 1622−1629.

(28) Buglio, D.; Palakurthi, S.; Byth, K.; Vega, F.; Toader, D.; Saeh, J.; Neelapu, S. S.; Younes, A. Essential role of TAK1 in regulating mantle cell lymphoma survival. *Blood* **2012**, *120*, 347−355.

(29) Totzke, J.; Gurbani, D.; Raphemot, R.; Hughes, P. F.; Bodoor, K.; Carlson, D. A.; Loiselle, D. R.; Bera, A. K.; Eibschutz, L. S.; Perkins, M. M.; Eubanks, A. L.; Campbell, P. M.; Fox, D. A.; Westover, K. D.; Haystead, T. A. J.; Derbyshire, E. R. Takinib, a Selective TAK1 Inhibitor, Broadens the Therapeutic Efficacy of TNF-*α* Inhibition for Cancer and Autoimmune Disease. *Cell Chemical Biology* **2017**, *24*, 1029−1039.

(30) Tan, L.; Nomanbhoy, T.; Gurbani, D.; Patricelli, M.; Hunter, J.; Geng, J.; Herhaus, I.; Zhang, J.; Pauls, E.; Ham, Y.; Choi, H. G.; Xie, T.; Deng, X.; Buhrlage, S. J.; Sim, T.; Cohen, P.; Sapkota, G.; Westover, K. D.; Gray, N. S. Discovery of type II inhibitors of TGF*β*-activated kinase 1 (TAK1) and mitogen-activated protein kinase kinase kinase kinase 2 (MAP4K2). *J. Med. Chem.* **2015**, *58*, 183−196.

(31) Goodnow, R. A., Jr.; Dumelin, C. A.; Keefe, A. D. Dna-encoded chemistry: enabling the deeper sampling of chemical space. *Nat. Rev. Drug Discovery* **2017**, *16*, 131−147.

(32) Imidazo[1,2-A]indeno[1,2-E]pyrazine-2-carboxylic acid derivatives, preparation thereof and drugs containing same. US5726175 A1, 1998.

(33) Wrobleski, S. T.; Lin, S.; Murali Dhar, T. G.; Dyckman, A. J.; Li, T.; Pitt, S.; Zhang, R.; Fan, Y.; Doweyko, A. M.; Tokarski, J. S.; Kish, K. F.; Kiefer, S. E.; Sack, J. S.; Newitt, J. A.; Mark, R.; Witmer, M. R.; McKinnon, M.; Barrish, J. C.; Dodd, J. H.; Schieven, G. L.; Leftheris, K. The identification of novel p38*α* isoform selective kinase inhibitors having an unprecedented p38*α* binding mode. *Bioorg. Med. Chem. Lett.* **2013**, *23*, 4120−4126.

(34) Röhm, S.; Berger, B.-T.; Schröder, M.; Chaikuad, A.; Winkel, R.; Hekking, K. F. W.; Benningshof, J. J. C.; Müller, G.; Tesch, R.; Kudolo, M.; Forster, M.; Laufer, S.; Knapp, S. Fast Iterative Synthetic Approach toward Identification of Novel Highly Selective p38 MAP Kinase Inhibitors. *J. Med. Chem.* **2019**, *62*, 10757−10782.